

# Infrared Thermography to Study Endwall Cooling and Heat Transfer in Turbine Stator Vane Passages Using the Auxiliary Wall Method.

by H. Werschnik\*, T. Ostrowski\*, G. Schmid\* and H.-P. Schiffer\*

\* Technische Universität Darmstadt, Institute of Gas Turbines and Aerospace Propulsion, Otto-Berndt-Straße 2, 64287 Darmstadt, Germany, werschnik@gr.tu-darmstadt.de

## Abstract

Experiments using the auxiliary wall method and infrared thermography allow to study film cooling and heat transfer in turbomachinery research with high spatial resolution. Using heater foils and pulse width modulation, an aluminum body is heated to constant wall temperature, controlled by thermocouples. The heat flux is then determined across a low conductivity layer of Ethylene-Tetra-Flour-Ethylene (ETFE), whereby 1-D conduction is assumed. Setting the base body to several quasi-steady wall temperatures allows to deduce adiabatic wall temperatures and heat transfer coefficients. Given a coolant and main flow with different temperature, cooling effectiveness can be calculated, using a superposition approach.

Experiments in the linear cascade test rig of the Institute for Gas Turbines and Aerospace Propulsion have been performed to study the effect of hub side coolant injection on the endwall heat transfer of a turbine stator row. The quality of results is examined through extensive data analysis, accompanied by a numerical simulation of the experiment.

## 1. Endwall Film-Cooling, Heat Transfer and Lean Combustion

Modern gas turbines and jet engines aim to increase the turbine inlet temperature, which is a consequence of the continuous strive to increase the overall cycle efficiency with a higher compressor pressure ratio. Being far higher than acceptable material temperatures this means, that the endwall of the first stator row requires efficient cooling techniques and the flow needs to be well-understood in terms of convective heat transfer. To reduce the flow temperature in the vicinity of the endwall, coolant air is injected through holes upstream of the first stator row. This coolant air can also act as a protective layer.

Endwall film cooling in axial turbines has been studied experimentally by Friedrichs [1]. He states three main

factors with influence on endwall heat transfer: The inlet temperature distribution, the thickness of the boundary layer and the three-dimensional flow field near the endwall. The latter is predominantly influenced by the secondary vortex system in a vane passage, which is also the crucial factor determining the endwall heat transfer, according to Han et. al. [2]. The model from Goldstein and Spores [3] illustrates this flow field (Figure 1) and mentions two dominating pressure gradients being responsible: The horseshoe vortex (1. & 2.) is induced by the stagnation pressure gradient in the incoming boundary layer, which is converted into a static pressure gradient when approaching leading edge of the vane. This forces the flow to turn towards the endwall and break up into two vortex structures. One leg is entering the passage along the suction side of the vane (2.) and the other along the pressure side of the vane (1.) with opposing rotational direction. The turning of the vanes induces the second important pressure gradient within the passage from the pressure side of the vane to the opposing suction side. A larger vortex structure starts to develop, denoted as the passage vortex (3.), where the pressure side leg of the horseshoe vortex encounters the vane surface, at its

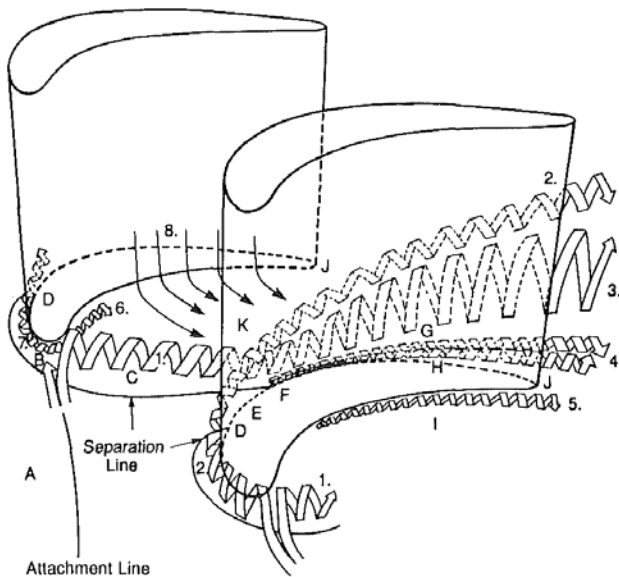


Figure 1: Vane passage vortex system from Goldstein and Spores [3]

shoulder, after travelling through the vane passage. The suction side leg of the horseshoe vortex remains close to the endwall up to a certain point, where it lifts off as well and starts to roll around the passage vortex with opposing rotational direction. Further low-momentum vortices develop at the airfoil corners (4., 5. and 6.), denoted as corner vortices. Horseshoe and passage vortex cause the formation of a three-dimensional separation line for the inlet boundary layer. Downstream of the separation line, a highly skewed new boundary layer begins to develop, fed by downwash from the vane's pressure side (8.). An attachment line divides fluid that enters one vane passage from the fluid entering the subsequent one. Where this line intersects the separation line, a saddle point is found. This vortex system is similar for all vane passages and determines heat transfer peak and minimum regions on the endwall. Friedrichs [1] gives an

overview of existing experimental work and states the common understanding of high heat transfer regions as shown in Figure 2.

According to Dückerhoff [4], a film cooling process is influenced by aerodynamic (density rate, blowing rate, turbulence level), geometric (hole geometry, angle and shape) and machine parameters (unsteady effects). Film cooling thereby has a large influence on the incoming endwall boundary layer, which can both be reenergized or weakened by the coolant injection and in this way influence the position of characteristic flow features and their effect on heat transfer. Aside from its effect on endwall heat transfer, film cooling also influences the aerodynamic losses in a stator passage: When injected upstream of the vortex lift-off line, the formation of the horseshoe-vortex and other secondary flow structures within the passage can be attenuated and their associated losses can be reduced according to Friedrichs [5] for certain blowing rates and injection geometries. Due to high losses within the injection holes themselves and mixing losses between coolant and main stream however, the overall losses are increased in any case. Coolant injection upstream of the separation line, as modeled in the present study can contribute in cooling a significant part of the endwall up to the separation line.

A driving factor for the research and work presented is the development of future aeroengine combustors which focuses on reducing pollutant emissions as well as increasing efficiency. Whereas a high turbine entry temperature is in favor of the latter, this increases the  $\text{NO}_x$ -emissions as well. Demanded by legislative requirements, a reduction is necessary instead according to Lazik et. al. [6]. This is hardly achievable with existing designs. The important factors of combustion temperature and reaction time have a major influence on the  $\text{NO}_x$ -level. The equivalence ratio has to be carefully selected: Whereas a low equivalence ratio has a positive influence on  $\text{NO}_x$ -emissions, it also has an adverse effect on flame stability and ignitability. To overcome this problem, a combustor concept known as lean combustion has been developed. Increased swirl in the combustion region is used to create a recirculation zone to stabilize a lean combustion.

From the point of view of turbine design, this however poses challenges: The increased combustor swirl is not fully attenuated until turbine inlet, and as a consequence affects turbine performance as well as cooling. Moreover, the temperature distribution is changed: A more homogenous distribution is created and hence higher air temperatures near the stator endwall occur. Therefore, its cooling is a crucial factor for the development of the lean combustion concept and needs to be accompanied by experiments on realistic combustor geometries. This underlines the need for the measurement technique presented in this work, which is developed to yield this data on 3D-shaped surface geometries and in a rotating annular rig.

## 2. Endwall Heat Transfer Measurement in Turbomachinery - An overview

There are various experimental methods to quantify convective heat transfer for flow situations with and without coolant injection of which a brief overview will be given.

The local heat transfer on a surface is physically depending on the temperature gradient within the boundary layer of the near-wall flow. Due to its small scale, this gradient is hard to measure experimentally, which is shown by Han and Goldstein [7]. They used a butt-welded small-scale thermocouple on a traversable mount to study thermal boundary layer profiles near a turbine stator endwall. The technique is limited by conduction errors in thin boundary layers and challenging since the probe is hard to position when the flow velocity is high.

Due to similar limitations, most methods determine the local heat transfer with a coefficient HTC, which compares the local heat flux resulting from a temperature difference between the wall and a certain reference temperature (Equation 1).

$$HTC(x) = \frac{\dot{q}(x)}{T(x) - T_{ref}} \quad (1)$$

Various heat transfer measurement techniques have been used to study vane endwall heat transfer with spatial resolution. Notable studies yielding surface heat transfer data for turbine endwalls include Blair et. al. [8],

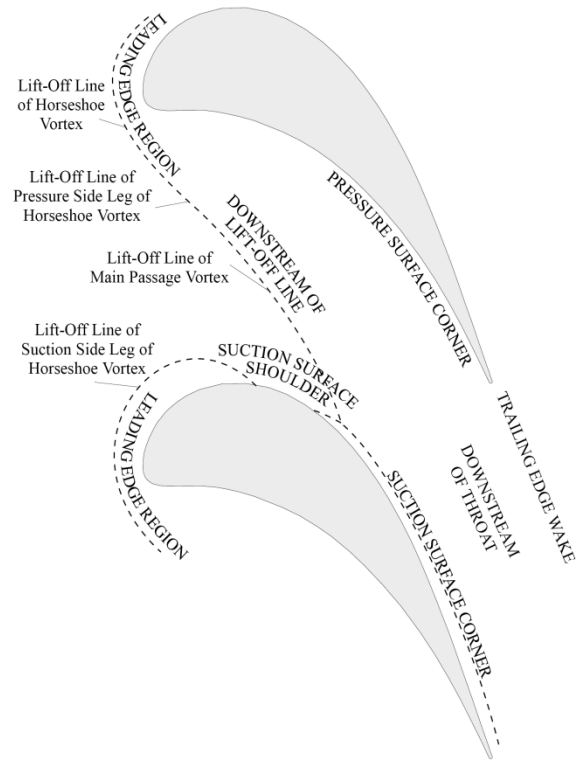


Figure 2: High endwall heat transfer regions according to Friedrichs [1]

Goldstein and Spores [2], Graziani et. al. [9] and Giel et. al. [10,11], among others. Blair et. al. [8] conducted research on local film cooling effectiveness and heat transfer values in a linear cascade. Goldstein and Spores used an indirect measurement method: The heat and mass transfer analogy with the naphthalene sublimation technique provides a way to acquire representative Stanton numbers for the whole endwall region between two turbine vanes. They discovered peak heat transfer regions and showed their correlation to the secondary vortex system in the passage. The importance of high resolution data for the interpretation of results was explained. Moreover, they further discovered evidence which helped in understanding the formation of the pressure side and suction side corner vortices. Airfoil and endwall heat transfer was also measured by Graziani et. al. [9] in a linear cascade using a direct measurement technique with a constant-heat-flux-approach on the surfaces of interest: Surface Thermocouples were placed on strip heaters to gain a high spatial resolution in expected areas of high heat transfer gradients. The study also shows the effect of the inlet boundary layer thickness: For a thin boundary layer, the three-dimensional separation line moves further down into the passage. The streamlines downstream of the separation line are nearly perpendicular to the endwall pressure field, whereas the heat transfer contours exhibit an angle to it. A low heat transfer region is discovered near the pressure side. All methods are a challenge for experimental work, since both the heat flux and the driving temperature gradient have to be measured and because of the limited accessibility in test rigs. Giel et. al. [10,11] studied heat transfer on turbine blades and endwalls, using a constant wall temperature approach. They applied thermochromic liquid crystals on well-conductive material, which was covered by a low-conductive material, yielding local heat transfer values with high resolution with the advantage, that conduction problems into the structure can be avoided.

A detailed overview of other direct heat transfer measurement techniques can be found in Kaiser [12].

### 3. Experimental Technique – the Auxiliary Wall Method

The presented experimental method uses a near adiabatic auxiliary wall, which is made of an insulating material. It covers a metal base material which is known to have a high coefficient of heat conduction. Copper or aluminum can be considered technically useful materials, since there is usually enough manufacturing experience and availability of these materials in machining shops. For the present study, an aluminum AlMgSi1 alloy with a thermal conduction coefficient of more than 150 W/(mK) has been used. The base material is heated to a constant temperature level using heater foils. Local differences in heat flux appear but are homogenized by the well conducting base material resulting in a near-uniform temperature distribution underneath the auxiliary wall. To define a local heat transfer coefficient, heat flux rates are calculated using the temperature gradient across the auxiliary wall (equation 2). Similar approaches to study turbomachinery heat transfer can be found in Giel et. al. [10,11], Martini et. al. [12] and Laveau et. al. [13].

The auxiliary wall is manufactured from ethylene tetrafluoroethylene (ETFE). This material has been chosen due to its glass transition temperature being out of the target temperature range for the experiments and its low thermal conductivity. The method assumes that the local heat flux being transferred from the wall into the flow has to pass through the wall itself before and that no significant conductive heat transport occurs within transversal direction in the auxiliary wall.

$$\dot{q}(x) = \frac{\lambda_{ETFE}}{l} (T_w(x) - T_{Al}) \quad (2)$$

The ETFE's thermal conductivity has been measured with a laser-response transition measurement. It has been determined to an average value  $\lambda_{ETFE}$  of 0.195 W/(mK) and shows only limited dependence to temperature. The absolute value is lower than in the literature for homogeneous ETFE materials. According to the laboratory of Netzsch [15], the manufacturing process and filling materials could be a reason. Since the specific heat is also determined to values below literature, the assumption is fortified. The ETFE is applied through electrostatic powder coating to the aluminum surface. Afterwards, the measurement area is machined to achieve a smooth surface and a layer thickness of 0.75-1 mm which is measured using a laser triangulation system with an accuracy of about 5 $\mu$ m. Finally, the surface is coated with black paint (Nextel Velvet Coating) with an emissivity value  $\epsilon$  of 0.97 according to Lohrengel [16].

Infrared thermography is used to determine the surface temperature distribution. An in-situ calibration of surface temperature values is performed: Reference thermocouples are positioned as close as possible underneath small steps the aluminum base material and not coated with ETFE, but only with black paint. The calibration curve is determined on the basis of Ochs et. al. [17]. A schematic of the experimental setup is depicted in Figure 4.

The infrared data is recorded using a FLIR X6540sc camera with an InSb-detector and a spectral response between 2,5 and 5,1 microns. The camera is placed above an uncoated ZnS-glass with a transmissivity  $\tau$  of 71-73 % in the detector range. A frame rate of 10Hz is used and hence during the 30s-sampling time, 300 thermograms are recorded with 640x512 pixels each. This results in a spatial resolution of at least 0,4mm on the measurement surface depending on viewing angles. Four overlapping camera positions have been used to cover the area of interest with a minimum of three reference positions in the field of view. In overlapping areas, an arithmetic average is calculated.

As a reference temperature for the heat transfer coefficient (ref. equation 1), the local adiabatic wall temperature is deduced according to Gritsch et. al. [18]. This requires various subsequent settings of steady wall temperatures and the corresponding local heat flux values. A linear regression then yields the local wall temperature where no heat flux

would occur (Figure 3). The heat transfer coefficient determined in this way is called adiabatic heat transfer coefficient and it will be used in the presentation of all results. Its significance is illustrated by Moffat [19].

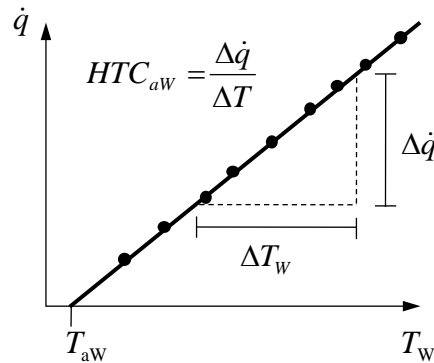


**Figure 3: Linear regression to deduce adiabatic heat transfer coefficient  $HTC_{aw}$**

Data is recorded for nine different heater settings, leading to base material temperatures between 333 K and 373 K. The temperature is controlled by pulse-width-modulation within a band of 0.1 K during data acquisition resulting in a quasi-isothermal distribution in the base material underneath the auxiliary wall.

One of the method's advantage is that it can also be applied to 3D-shaped surfaces. This enables to study engine-realistic combustor-turbine interfaces, with a tapered annulus geometry. The future Large Scale Turbine Rig (LSTR) at TU Darmstadt will offer this possibility and use the presented method to study the aero-thermal interaction of combustor and turbine with varying inflow conditions, also including a lean combustion aerodynamic (cold) setup. The instrumentation carrier for the campaign is currently being manufactured and measurements are expected to begin in the fall of 2014. Numerical Simulations of the planned measurement campaign at the LSTR have been conducted by Schmid et. al. [20]

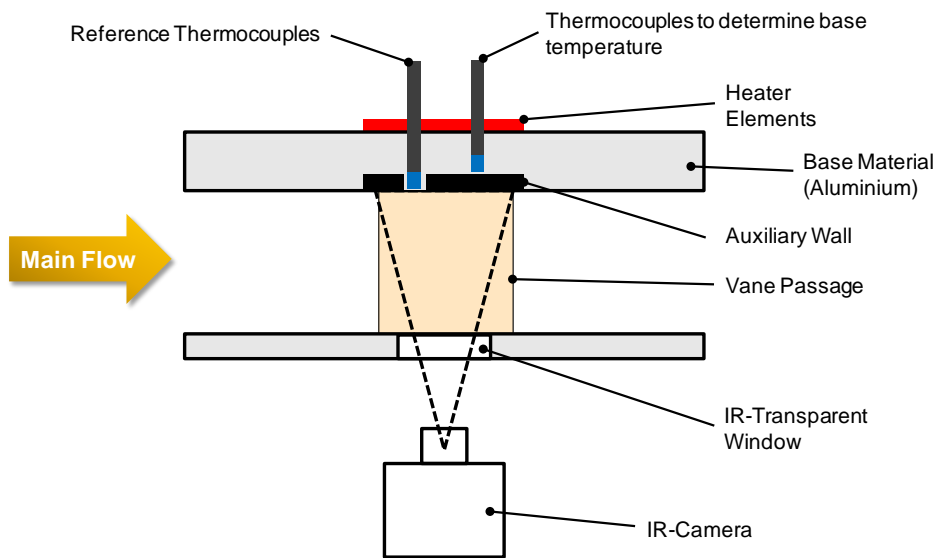


**Figure 4: Schematic of the experimental setup**

#### 4. Description of the Test Rig and Experiments

The measurements were carried out at the low speed linear cascade test rig at the Institute of Gas Turbines and Aerospace Propulsion, Technische Universität Darmstadt (Figure 5). The rig is operated in suction mode and controlled to a constant Reynolds number of 100,000. The test section is made up of five cascade vanes, whereas the upper endwall between two of the centered vanes is instrumented for heat transfer measurements as described in section 3. A coolant injection module allows varying both injection rate and geometry upstream of the stator vanes. Two configurations have been studied: A baseline case without coolant injection and a cooled case with a series of 20 holes per stator passage with a diameter of 4mm each and a hole spacing of 10mm. The coolant is introduced with a stream wise inclination of 45°. The aerodynamic cooling parameters have been varied as shown in Table 1, the definitions are stated in equation 3. Data for the settings in bold have been recorded for the whole endwall whereas for the three remaining settings, only the leading edge regions has been observed. The thermo-optical access is positioned on the

opposing side. The camera is mounted on a rack allowing accurate adjustment of the field of view towards the passage endwall. A more detailed description of the test rig can be found in Giller et al. [21], the corresponding numerical work in Schmid et. al. [22]

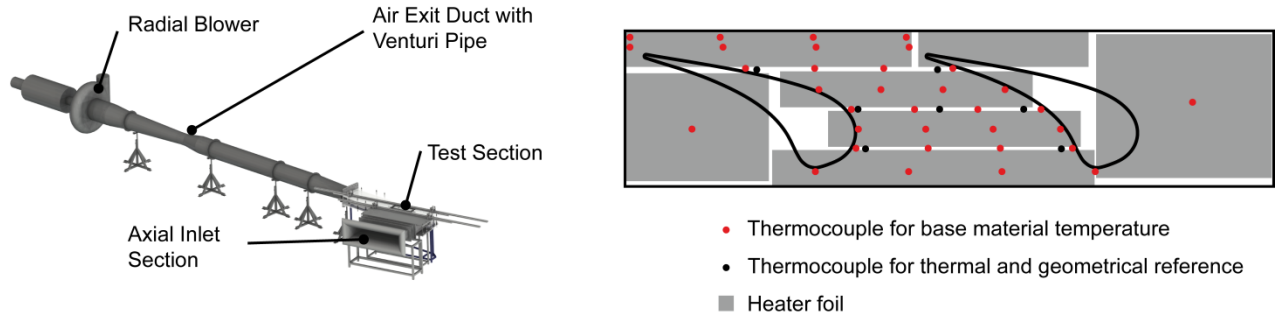


**Figure 5: Test rig setup and instrumentation diagram**

To monitor the base material temperature, an array of 32 thermocouples has been installed, with 7 additional thermocouples representing thermal and geometrical reference values for the infrared image. The positions are shown in Figure 5. Seven heater foils are individually controlled to introduce the heat flux and to keep the base material at a homogenous temperature level within a band of 0.5 K.

**Table 1: Aerodynamic film cooling parameters**

Injection rate IR [% Mainflow]	Blowing ratio M [-]	Density ratio DR [-]	Reynolds number [-]
0	-	1.0	100,000
1.6	2.6		
2.4	3.9		
3.7	6.1		
5.0	8.2		

$$M = \frac{\rho_{cool} \cdot u_{cool}}{\rho_{\infty} \cdot u_{\infty}}, \quad IR = \frac{\dot{m}_{cool}}{\dot{m}_{Main}}, \quad DR = \frac{\rho_{cool}}{\rho_{\infty}} \quad (3)$$

The coolant injection module in the present investigation is designed to model hub side coolant injection at the interface of combustor and turbine sections in modern gas turbines. High mass flow rates and blowing rates are realized. In former engine designs, this coolant air flow has mainly been dedicated to reduce the air temperature in the vicinity of the endwall to lower the amount of heat flux into the structure and to seal the combustor turbine interface gap. Current research by Knost et. al. [23] shows, that it can also have a significant cooling effect on parts of the endwall.

## 5. Endwall Heat Transfer Results

Figure 6 shows the heat transfer coefficient averaged in pitch wise direction - normal to the inflow direction - over the relative axial position in respect to the vane's axial chord length for both cases. Due to limitations in the optical access, the endwall between two vanes was fully covered up to an  $x/c_{ax}$  of 0.9.

For the uncooled case, the heat transfer coefficient yields the typical characteristics for a NGV passage: There is an intermediate peak upstream of the leading edge at  $x/c_{ax}$  of -0.01 due to the influence of the vortex system ahead of the stator stage, namely the formation of the horseshoe vortex. Within the passage, the growing inlet boundary layer causes a decreasing heat transfer coefficient. The newly formed thin boundary layer after the separation line increases the heat transfer coefficient at about mid-passage towards the exit of the vane passage reaching values as high as at the

intermediate peak upstream of the leading edge. Since the measurement area is thermally decoupled from the remainder of the test rig, a step change in heat flux occurs at its onset and the thermal boundary layer starts to form at  $x/c_{ax}$  of -0.2.

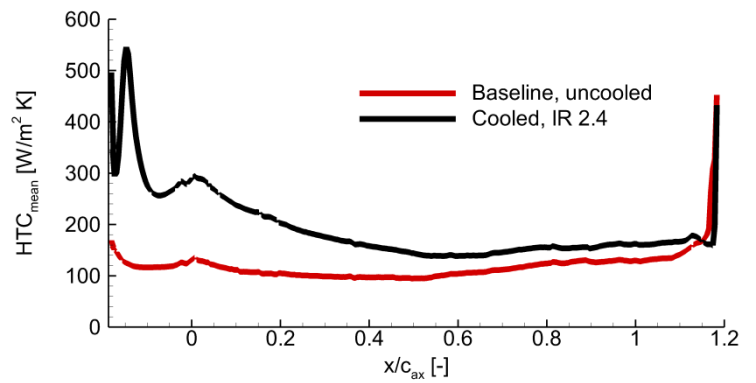


**Figure 6: Endwall heat transfer, averaged in pitch wise direction**

The coolant injection increases heat transfer throughout the whole passage. However, the dominant effect occurs from the leading edge up to about mid-passage. The characteristic intermediate peak upstream of the leading edge remains but is shifted into the passage to a  $x/c_{ax}$  of 0.03, i. e. slightly beyond the leading edge. The formation of the horseshoe vortex seems to be influenced and its effect on heat transfer shifted into the passage. The heat transfer coefficient decreases steeper as for the uncooled case towards mid-passage. The change to increasing characteristics begins further downstream in the passage at about  $x/c_{ax}$  of 0.65. Thereafter, the characteristics follow that of the uncooled case almost with the same slope, but with a constant offset of about 50 W/(m<sup>2</sup>K). Towards the physical end of the measurement area, the heat transfer coefficient heads for infinity in both cases.

Figure 7 shows the local distribution of the experimental results. The inflow direction in all contour plots is from bottom to top.

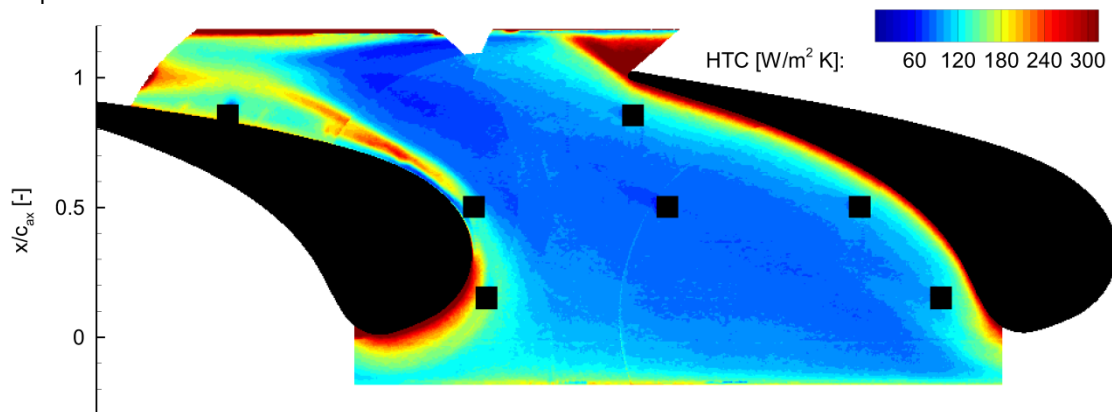


**Figure 7: Endwall heat transfer distribution for the baseline case**

Local maxima for the heat transfer coefficient are identified as follows: A peak is found in the leading edge region of the airfoil where a new boundary layer is formed after the lift-off of the horseshoe vortex system. Near the pressure and suction side corners of the vane the thin boundary layer and high velocities increase heat transfer. The dominating heat transfer peak starts near the shoulder region of the vane suction side, a reason of the interaction of secondary vortices and high velocities. The last peak is found on the suction side endwall portion downstream of the trailing edge. A possible explanation for this peak is a flow separation near the endwall. The vane configuration in the test rig seems to be susceptible to separation seems to be susceptible to separation even for small incidence angles. In contrast, the CFD simulation which have been conducted to support this investigation did not predict a separation on the vane suction side. Therefore, the maximum in HTC in the rear part of the vane suction side and down to the trailing edge is not present in the computational results. Excluding the latter, all regions have been mentioned by previous experiments as regions of high heat transfer. The typical heat transfer distribution seen in the literature with lower heat transfer coefficients upstream of the separation line and high value downstream of it, is not found in the experiments. Whereas in the vicinity of the vanes, the distribution is similar to literature data, the heat transfer coefficient distribution in the center of the passage is more similar to a flat plate in turbulent inflow.

Local heat transfer is drastically increased downstream of the coolant injection: Figure 8 shows the local distribution for an IR of 2.4. A smaller maximum is found downstream of the injection holes. Maxima with larger extension are located between adjacent holes and further downstream into the passage. This is one indication, that the coolant jets do not stay attached to the endwall. The endwall shows a heat transfer distribution found in the literature [4] for moderate to high blowing rates in coolant injection cases, typical for vortex shedding off a jet-in-crossflow. In general and especially

for high blowing rates, the coolant jet acts similar to a cylinder in crossflow, creating several vortex pairs downstream of the jet.

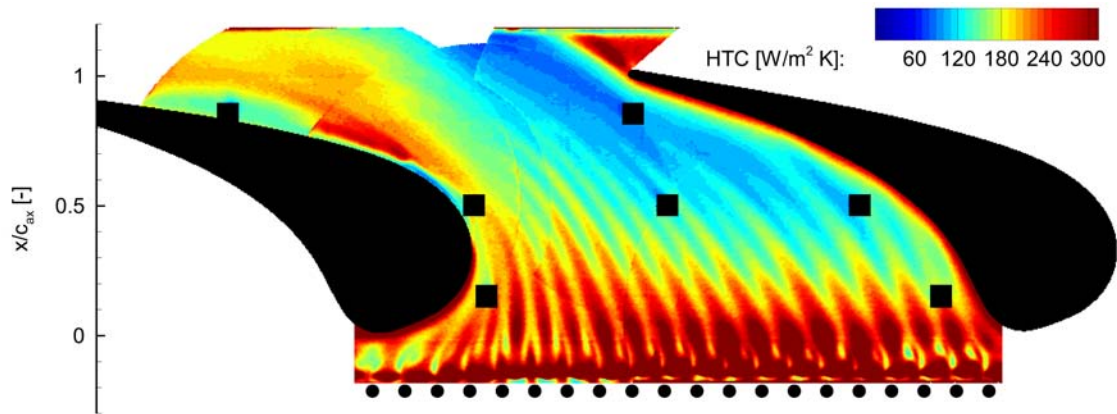


**Figure 8: Endwall heat transfer distribution for the cooled case (IR 2.4)**

The dominant maximum from the baseline case near the suction side downstream of the vane's shoulder can be found in a similar position for the cooled case, but with less distinct maximum values and an increased spatial distribution. To examine the method's sensitivity to flow field changes, the coolant massflow and blowing rate of the coolant injection has been varied as mentioned in Table 1. Results are shown for the leading edge region in Figure 9.

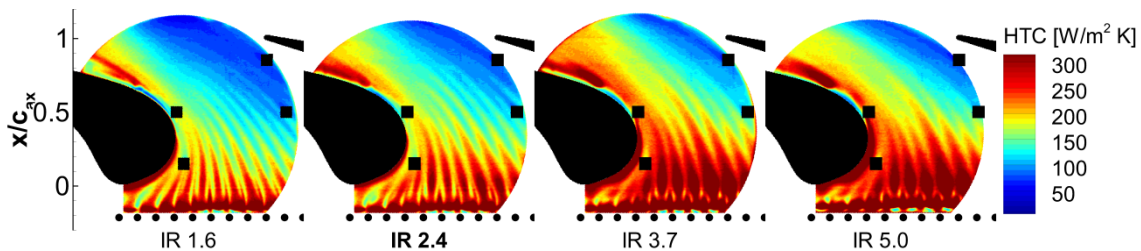


**Figure 9: Heat transfer in the leading edge area for varied injection rates**

It can be seen, that for all four cases, heat transfer peaks are located downstream of the region between adjacent injection holes but not downstream of the holes themselves. The region with higher level heat transfer is increased with the injection rate. For the IR of 5.0, no significant further change occurs compared to the next smaller IR. The location and direction of the increased heat transfer contours does not differ due to the blowing rate. Together with the observations before, this suggests that the coolant does not attach to the wall but protrudes through the boundary layer for all blowing rates. This result could be confirmed qualitatively by a CFD simulation for which a structured mesh of the cooling holes penetrating into the hub boundary layer was generated.

## 6. Numerical Simulations - Setup and Results

One passage of this turbine cascade is modelled numerically with the commercial CFD solver FINE/Turbo for comparison with experimental data. A block-structured mesh of 4.9M nodes is generated with AutoGrid. The boundary layer is resolved by at least ten cells keeping the normalized wall distance of the first cell  $y^+$  below unity and the expansion ratio below 1.5. Hence, the turbulence model by Spalart and Allmaras is applied without any wall functions. For the computation of heat transfer coefficient, a constant wall temperature is specified. The resulting heat flux is normalized using the difference of this wall temperature and the total temperature at the inlet of the cascade. The end wall film cooling is included applying a source term model with the measured cooling mass flow rate and temperature as boundary condition.

Both cases studied in the experiment have been simulated. The overall level of heat transfer is underpredicted by the numerical simulation. This might be due to the source term model which is used for film cooling. This model distributes the cooling mass flow onto several cells at the hub end wall which coincide approximately with the location of a cooling hole. Thus, the coolant injection does not include any velocity gradients of a boundary layer which would form inside a cooling hole. In order to obtain a more accurate result of the film cooling injection, the cooling hole geometry needs to be meshed resolving the boundary layer inside the holes. This requires a non-matching connection of the cooling hole geometry and the main passage or alternatively an unstructured mesh. All these options are investigated in terms of accuracy and computational cost. For the current investigation, the source term model was preferred which

allows a fast and robust computation of several operating conditions. The mesh of the main channel remains unchanged which is crucial to obtain good results inside the cascade passage.

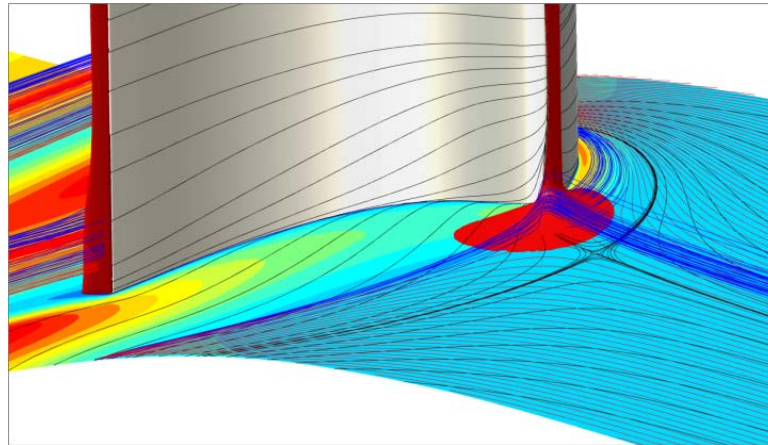


**Figure 10: Numerical simulation for the baseline case**

Figure 10 shows this passage looking on the pressure side of the vane. The colour contour on the hub represents the heat transfer coefficient for the baseline case showing a pronounced maximum on the suction side near the leading edge and in the rear parts of the vane on the pressure side. The streamlines in blue represent the incoming boundary layer which is turned at the leading edge into the horseshoe vortex. The flow of negative axial velocity is marked by a red iso surface near the leading edge. The suction side leg of the horseshoe vortex drives fluid downwards from the vane onto the hub end wall. The main flow velocity at the vane shoulder is very high causing the maximum in HTC at this location. The pressure side leg of the horseshoe vortex as well as the incoming boundary layer (red streamlines) are shifted towards the opposite suction side by the passage cross flow. This flow can be identified by end wall streamlines of viscous stress which are marked in black in this Figure. The passage cross flow causes a down wash of fluid on the vane pressure side which decreases the boundary layer thickness and hence, leads to the maximum of HTC near the vane trailing edge. The qualitative prediction of the secondary flow structures and the result in heat transfer is in good agreement with the description by Friedrichs [1] shown in Figure 2. Only in the rear part of this cascade, the area of low HTC upstream of the separation line of the pressure side leg of the horseshoe vortex does not end on the opposite suction side but propagates further downstream to the exit of the passage. This might be due to the operation conditions of this cascade. The heat transfer coefficients for varied inflow rates are shown in Figure 11.

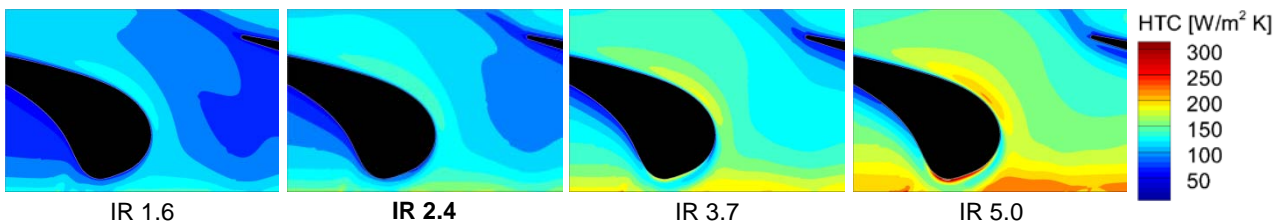


**Figure 11: Heat transfer coefficient for varied injection rates, numerical simulation**

## 7. Quality of Results

A 2-D FEM using COMSOL Multiphysics was performed in the high-gradient area downstream of the trailing edge with the experimental data for the heat transfer coefficient and the temperature distribution below and above the auxiliary wall. Planar heat conduction within the ETFE coating was observed, but had no significant effect on normal heat conduction within the auxiliary wall. Thus, no significant change in the heat transfer coefficient contours is observed. Since measured temperature differences are slightly attenuated in high gradient areas, it is planned to conduct three-dimensional-FEM calculations for future investigations to further improve measurement accuracy.

## 8. Conclusion and Outlook

A method has been developed to study local heat transfer coefficients on turbine stator endwalls. The use of a powder coated and machined auxiliary wall enables the use of this measurement technique also on 3D-shaped surfaces. To validate the technique, measurements have been conducted at a linear cascade rig. Heat transfer has been studied for an uncooled baseline case as well as for a second case with hub side coolant injection upstream of the leading edge.

Heat transfer peaks are determined upstream of the leading edge, near the vane's pressure side and suction side corners, downstream of the trailing edge and a dominant maximum near the suction side shoulder section of the endwall. The maximum downstream of the trailing edge is thought to result from a flow separation. All other maxima are usually found in the literature as well.

Coolant injection increases heat transfer on the endwall. The increase is greater near the injection holes and for higher injection rates. The peaks in the leading edge region and near the suction side shoulder of the vane are also found for the cooled case with increased spatial distribution.

A numerical simulation of the experiment is used to relate the results to the flow field phenomena in the test rig. They show that the cascade rig is susceptible to flow separation near the suction side of the endwall. The coolant flows are not attached to the endwall. The results for the uncooled case are comparable to the experimental results, however maximum downstream of the trailing edge is not observed. The heat transfer level is underpredicted in the numerical simulation.

The results show the current state of the data analysis tools. In the future it is planned to further optimize the geometrical and thermal calibration processes. Further data on the aerodynamic flow field will accompany the thermal measurements to acquire a deeper insight into the flow features which influence endwall heat transfer.

The method itself will be used for future experiments in a rotating turbine rig and with more realistic geometries of the combustor-turbine interface in aeroengines with variable inflow conditions. The instrumentation carrier is currently manufactured and prepared for the measurement campaign, that is scheduled to begin in the fall of this year.

## Acknowledgments

The work reported was partly funded within the framework of the "AG Turbo" by the "Bundesministerium für Bildung, Wissenschaft, Forschung und Technologie" (FKZ: 03ET2013K) as well as by Rolls-Royce Deutschland GmbH and ALSTOM Power. The contribution of Marcel Adam and Lars Ohde is gratefully acknowledged.

## 9. References

- [1] Friedrichs, S. "Endwall Film-Cooling in Axial Flow Turbines", Dissertation, University of Cambridge, 1994.
- [2] Han, J.-C., Dutta, S., Ekkad, S. "Gas Turbine Heat Transfer and Cooling Technology", 2002.
- [3] Goldstein, R.J., Spores, R.A., "Turbulent Transport on the Endwall in the Region Between Adjacent Turbine Blades", ASME J. Heat Transfer, Vol. 110, 1988.
- [4] Dückershoff, R. "Filmkühlung in Gebieten mit verzögerter Hauptströmung und in Bereichen lokaler Strömungsablösung", Dissertation, BTU Cottbus, 2004.
- [5] Friedrichs, S., Hodson, H.P., Dawes, W.N. "Aerodynamic Aspects of Endwall Film-Cooling", ASME J. Turbomach., Vol. 119, 1997.
- [6] Lazik, W., Doerr, T., Bake, S., v.d. Bank, R., Rackwitz, L. "Development of Lean-Burn Low-NO<sub>x</sub> Combustion Technology at Rolls-Royce Deutschland", ASME Turbo Expo 2008, GT2008-51115.
- [7] Han, S. and Goldstein, R.J., "Heat Transfer Study in a Linear Turbine Cascade Using a Thermal Boundary Layer Measurement Technique", ASME J. Heat Transfer, Vol. 129, 2007.
- [8] Blair, M. F., "An Experimental Study of Heat Transfer and Film Cooling on Large-Scale Turbine Endwalls", ASME J. Heat Transfer, Vol. 96, 1974.
- [9] Graziani, R.A., Blair, M.F., Taylor J.R., Mayle, R.E., "An Experimental Study of Endwall and Airfoil Surface Heat Transfer in a Large Scale Turbine Blade Cascade", ASME J. Eng. Gas Turbines Power, vol. 102, 1978.
- [10] Giel P.W., Van Fossen G.J., Boyle R.J., Thurman D.R., Civinskis K.C. "Blade Heat Transfer Measurements and Predictions in a Transonic Turbine Cascade" NASA/TM-1999-209296, 1999.
- [11] Giel, P. W., Thurman, D.R., Van Fossen, G.J., Hippensteele, S.A., Boyle, R.J. "Endwall Heat Transfer Measurements in a Transonic Turbine Cascade", NASA-TM-107387, 1996.
- [12] Martini P., Schulz A., Bauer H.-J. "Film Cooling Effectiveness and Heat Transfer on the Trailing Edge Cutback of Gas Turbine Airfoils with Various Internal Cooling Designs" ASME J. Turbomach., Vol. 128, 2006.
- [13] Laveau B., Abhari R., Crawford, M.C., Lutum, E. "High-Resolution Heat Transfer Measurements on Flat and Contoured Endwall in a Linear Cascade", ASME Turbo Expo 2012, GT2012-69737.
- [14] Kaiser E., "Zur Wärmestrommessung an Oberflächen - unter besonderer Berücksichtigung von Hilfswand-Wärmestromaufnehmern". Technische Universität Dresden, Dissertation, 1981.
- [15] Netzsch Applikationslabor, "Thermophysikalische Eigenschaften von ETFE", 2013.
- [16] Lohrengel J., Todtenhaupt R. "Wärmeleitfähigkeit, Gesamtemissionsgrade und spektrale Emissionsgrade der Beschichtung Nextel-Velvet-Coating 811 (RAL 900 15 tiefschwarz matt)" PTB-Mitteilungen 106 (1996)
- [17] Ochs M., Horbach T., Schulz A., Koch R., Bauer H.-J. "A Novel Calibration Method for an Infrared Thermography System applied to Heat Transfer Experiments" Meas. Sci. Technol. 20, 2009.

- [18] Gritsch M., Baldauf S., Martiny M., Schulz A., Wittig S., "The Superposition Approach to local Heat Transfer Coefficients in High Density Ratio Film Cooling Flows". ASME Turbo Expo 1999, 99-GT-168.
- [19] Moffat R. J., " $h_{\text{adiabatic}}$  and  $u'_{\text{max}}$ ", ASME J. Electronic Packaging, Vol 126, 2004.
- [20] Schmid G., Krichbaum A., Werschnik H., Schiffer H.-P., "The Impact of Realistic Inlet Swirl on a 1 1/2 Stage Axial Turbine", Proceedings of the ASME Turbo Expo 2014, GT2014-26716.
- [21] Giller L., Schiffer H.-P. "Interactions between the Combustor Swirl and the High Pressure Stator of a Turbine", ASME Turbo Expo 2012, GT2012-69157.
- [22] Schmid G., Schiffer, H.-P. „Numerical Investigation of Inlet Swirl in a Turbine Cascade“, ASME Turbo Expo 2012, GT 2012-69397.
- [23] Knost, D.G., Thole, K.A. "Adiabatic Effectiveness Measurements of Endwall Film-Cooling for a First-Stage-Vane", ASME J. Turbomach., Vol. 127, 2005.